



Paper Type: Original Article

## Featural Analysis, Protective Capacity and Potential of Shallow Hydrogeological Layers of Densely Populated Residential Area, Akwa Ibom State, Southern Nigeria

Kufre R. Ekanem<sup>1\*</sup>, Udeme U. Inyang<sup>1</sup> , Nsidibe N. Okonna<sup>1</sup> 

<sup>1</sup>Department of Science Technology, School of Applied Sciences, Akwa Ibom State Polytechnic, Ikot Osurua, Akwa Ibom State, Nigeria; ekanemkufre03@gmail.com; ekanemkufre03@gmail.com; udemeinyang655@gmail.com; Nsidebeabasiokonna@yahoo.com.

### Citation:

Received: 12 February 2024

Revised: 2 April 2024

Accepted: 2 June 2024

Ekanem, K. R., Inyang, U. U., & Okonna, N. N. (2024). Featural analysis, protective capacity, and potential of shallow hydrogeological layers of densely populated residential area, Akwa Ibom State, Southern Nigeria. *Optimality*, 1 (1), 46-65.


### Abstract

Geoelectrical Resistivity Technology (GRT) and geological data were employed to delineate the hydrokinetic characteristics, protective capacity, and groundwater potential of a sought-after housing development in Southern Nigeria. The GRT utilized Schlumberger's 1-D Vertical Electrical Sounding (VES) resistivity and 2-D Electrical Resistivity Tomography (ERT) techniques. The primary and secondary geo-electric indices were combined with existing geological data to calculate hydrodynamic parameter maps of the shallowest aquifer unit. These maps are crucial for effectively managing the unconfined aquifer system beneath, which is extensively utilized in the area. The study area's saturation dynamics were determined by analyzing total porosity (ranging from 0.282 to 0.691), specific yield (ranging from 0.040 to 0.107), field capacity/specific retention (ranging from 0.242 to 0.623), and storage-dependent drainability efficiency (ranging from 7.6% to 40.5%). The results indicated that the area experiences the most effective release of pore water when the drainability efficiency, which relies on storage, exceeds 21%. The range of potential index parameters, including Transmissivity (T) (57.4–4339.2 m<sup>2</sup>/day), Transverse Resistance (TR)/aquifer potential scale (453.6–152,756.5 Ωm<sup>2</sup>), permeability (91.7–7269.7 mD), and hydraulic conductivity (57.4–4339.2 m/day), exhibited favourable potential but limited to moderate protection, as indicated by the longitudinal conductance index (0.004–0.6218 Siemens). Given the strong preference of many people to live in this rapidly growing and competitive housing estate, it is important to establish effective waste disposal systems to prevent the leakage and infiltration of harmful substances, such as leachates and other organic/inorganic waste, into the vulnerable underground water sources that provide water for various purposes.


**Keywords:** Hydrokinetic properties, Parametric characterization, GRT, VES, SDE.

## 1 | Introduction

Shallow sedimentary hydrogeological units play a crucial role in storing groundwater at both regional and local levels. However, obtaining reliable hydrogeological data to effectively understand their distribution and

 Corresponding Author: ekanemkufre03@gmail.com



 Licensee System Analytics. This article is an open access article distributed under the terms and conditions of the Creative Commons Attribution (CC BY) license (<http://creativecommons.org/licenses/by/4.0>).

hydraulic properties can be challenging, costly, and time-consuming. Accurate knowledge of hydraulic parameters, including porosity, hydraulic conductivity, permeability tortuosity, specific yield, and specific retention, is essential for assessing the resources of a groundwater system. These parameters help evaluate the potential, protectivity, and vulnerability of the system to contamination, which are all crucial factors in targeted integrated water management [1]–[5]. Porosity is a hydrokinetic feature of a hydrogeological unit that represents the void space ratio in a particular volume of soil or rock sample to its total volume. It is typically stated as a percentage [6], [7]. Voids, pore spaces, and cracks are crucial in hydrodynamic investigations and parametric characterization in hydrogeology and hydrogeophysics. According to Fetter [8], soil moisture and groundwater are found in the empty spaces within the solid earth. It dictates how pollutant plumes are spread in interconnected pore networks. The hydrodynamic properties of rocks and soils on Earth, such as total porosity ( $\epsilon$ ), depend on factors such as the geometry, extent of voids, arrangement of grain sizes, and interconnectedness of the pores. These properties determine how water accumulates and passes through the material [9], [10].

According to Mazáč et al. [11], the size of grains does not affect the overall porosity in sediments of the same size. However, porosity changes depending on how the grains are packed together, and it can decrease as the particle size increases. According to Schwartz and Zhang [12], specific yield, also referred to as effective porosity or gravity water porosity, is a measure of the storage capacity of an open aquifer. It represents the ratio of the volume of water drained by gravity from saturated rock or soil to the total volume of the rock or soil [13].

Specific yield complements specific retention/field capacity in determining the total porosity of the aquifer. In the theory of aquifer systems, the drainable porosity is a storage coefficient that considers the impact of the unsaturated zone on water table dynamics. Typically, this coefficient is assumed to be constant. However, surficial and open aquifers' value is determined by the water table's depth and the geological unit's water retention characteristics [14]. The specific retention can be defined as the ratio of the volume of water in a rock or soil sample to the overall volume of the rock or soil. It represents the empty areas that generate water for wells and show great potential in supplying water to wells. Specific yield is a proportion of the total porosity of a porous media. The total porosity, which refers to the overall volume of pore space in a geologic unit, is significantly greater than the particular yield. Total porosity encompasses both the effective porosity, which refers to the interconnected portion of pore space, and the porosity resulting from isolated pores. The effective porosity encompasses both specific yield and specific retention.

Specific retention refers to the amount of water retained within a hydrogeological unit due to capillary forces and adhesion when emptying. The specific yield refers to the substantial quantity of water readily accessible for groundwater extraction when the water table is lowered, resulting in the drainage of porous materials. The soil water retention curve is a tool that quantifies the relationship between the water content of the soil and the capillary pressure it exerts. This relationship is influenced by both climatic conditions and the velocity of water flow at the pore scale, which is determined by the specific yield and retention capacity [15]. These factors are valuable for calculating the capacity of water pumps for various aquifer units using the storage-dependent drain ability efficiency tool, which is the ratio of specific yield to specific retention. The methods commonly employed to investigate specific yield, as outlined by Todd [16], include pumping, field saturation, recharge analysis, particle density measurement, and sampling following water table decline.

Nevertheless, Hamill and Bell [17] and George et al. [10] state that these methods require a significant investment of resources, including equipment, borehole data, and a substantial workforce, due to each methodology's complex and labour-intensive nature. From an economic standpoint, the geo-sounding technique has been demonstrated to be an effective method for assessing the structure, vulnerability, and potential of underground hydrogeological units in both large and medium-sized study areas [18]–[21].

Geo-sounding technologies operate under the assumption that the rock/soil matrix is primarily an insulating material. It can conduct an electric current when water or moisture is present in its pores [22], [23]. The skilful application of geo-sounding techniques by numerous researchers has enabled the production of reliable

evidence that revealed both qualitative and quantitative estimates of transmitting variables of hydrogeological units [23]–[26]. The effectiveness of studying hydrogeological units' parametric characteristics, protective nature, and potential can be enhanced by analyzing the spatial distribution of aquifer system indices on maps. This approach has been explored in many studies conducted by Stempvoort and Wassenaar [27], Aweto [28], Karadavut [29], and Shamsudduha et al. [30]. This paper investigates the estimates of primary and secondary geo-electrical attributes obtained through geo-electrical resistivity technology and other hydrogeological variables such as specific yield and retentive retention. The goal is to characterize a medium-sized housing estate and assess the protectivity, vulnerability, and potential of shallow groundwater resources that the estate's residents heavily abstract.

## 1.1 | Description of the Study Area

### 1.1.1 | Site location

Shelter Afrique, a moderately sized housing development, is situated in the mid-western region of Akwa Ibom State, located in Southern Nigeria. The majority of its land area is in Ibesikpo County, with a smaller section in Uyo County (Fig. 2). The occupied territory spans from latitudes 4.958° to 4.9917°N and longitudes 7.9417° to 7.9750° E, with an approximate area of 30.8 square kilometres. The region is characterized by a flat terrain, with altitudes ranging from a low point of 54 meters to a high point of 68 meters above sea level. The average elevation is 59 meters, as shown in Fig. 1.

The study area is a recently constructed and quickly growing residential area in the Uyo Senatorial District. It is home to past and current governors, deputy governors, members of the political class, and other influential individuals from Akwa Ibom State, as well as other states in Nigeria and those living abroad. Due to its medium size, the area is characterized by a high population density of individuals and physical infrastructure.

The region experiences a semi-temperate climate characterized by distinct dry and wet seasons. The dry season lasts from April to September, while the wet season occurs from October to March. The entire catchment area is affected by the tributaries of the enyiong river, which is the primary source of perennial surface water in Itu County. The temperature ranges from 26 to 32 °C, while the annual rainfall varies from 200 to 250 cm [21].

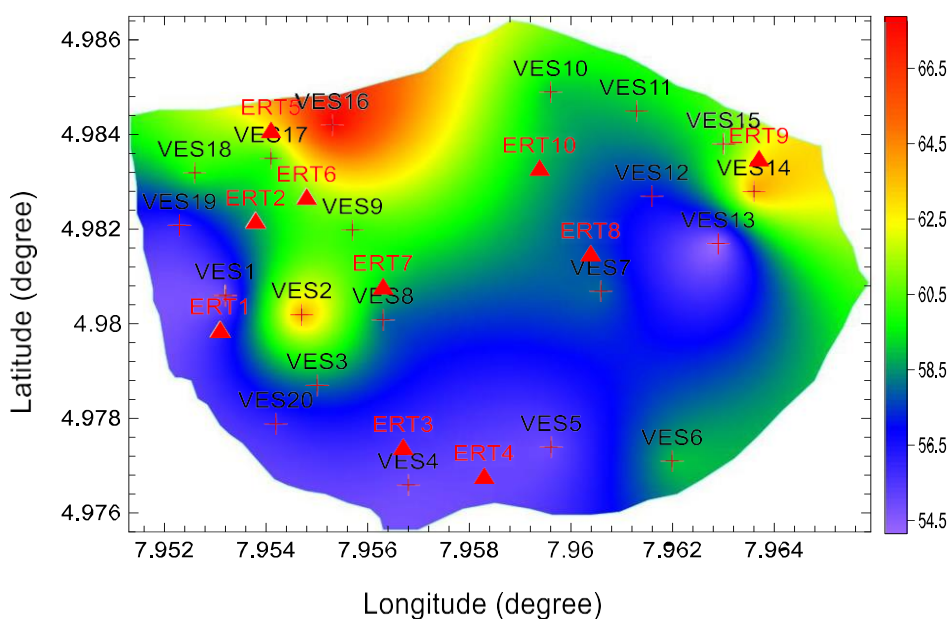
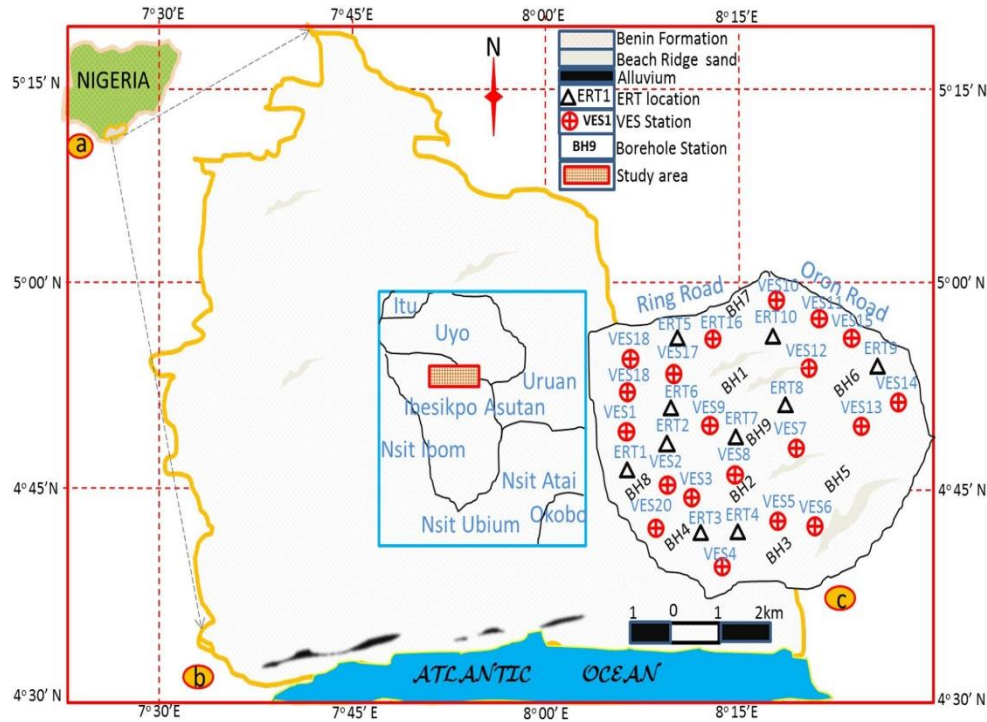


Fig. 1. Elevation map of the study area showing the topography of the study area.



**Fig. 2.** Schematic map of Nigeria; a. Schematic map of Nigeria showing the geographic location of Akwa Ibom State in Southern Nigeria, b. map of Akwa Ibom State showing the Atlantic Ocean and the geographical settings of the study area, c. geographic and model domain map showing geology, VES points and Boreholes.

## 1.2 | Geology of the Study Area

The groundwater extraction in the studied region occurs within the Youngest Continental Plain sand/Benin Formation of the Niger Delta in Southern Nigeria. The Benin Formation, which consists of alternating layers of sandstones and small amounts of claystone, is located above the Agbada Formation and Akata Formation in a specific order of burial depth [31], [32]. The research region is located in Southern Nigeria, as indicated by the Geological Survey Map series of Nigeria on sheets 79 for Umuhia and 82 for Calabar, with a scale of 1:250,000.

Benin Formation is often called Coastal Plain Sand [33]. Specifically, the area is predominantly located within the Benin Formation and partially within the Beach Ridge Complex and Alluvium of the Quaternary Period, as seen in *Fig. 2*. The composition of alluvial sands ranges from fine to coarse-grained sands (*Fig. 3*), whereas the light grey argillites are relatively little in quantity and scattered irregularly. Following rainfall, it is occasionally observed that sedimentation, erosion, and morphological differences occur in the surface layers. The alluvial sediments consistently occur at lower elevations and are attracted by gravity. The alluvial grains, characterized by a greyish hue, exhibit a characteristic texture that varies from fine to coarse, with alternating intercalations, as described by Short and Stauble [34] in 1967. The presence of groundwater in the area is influenced by various geological factors, including the structure, disturbances in the stratigraphy, and the arrangement of hydrogeological units [35], [36]. The hydraulic interconnections between the seasonal reduction in water levels and the groundwater level or the topography of groundwater conduits determine the depth and shape of wells and water bodies.



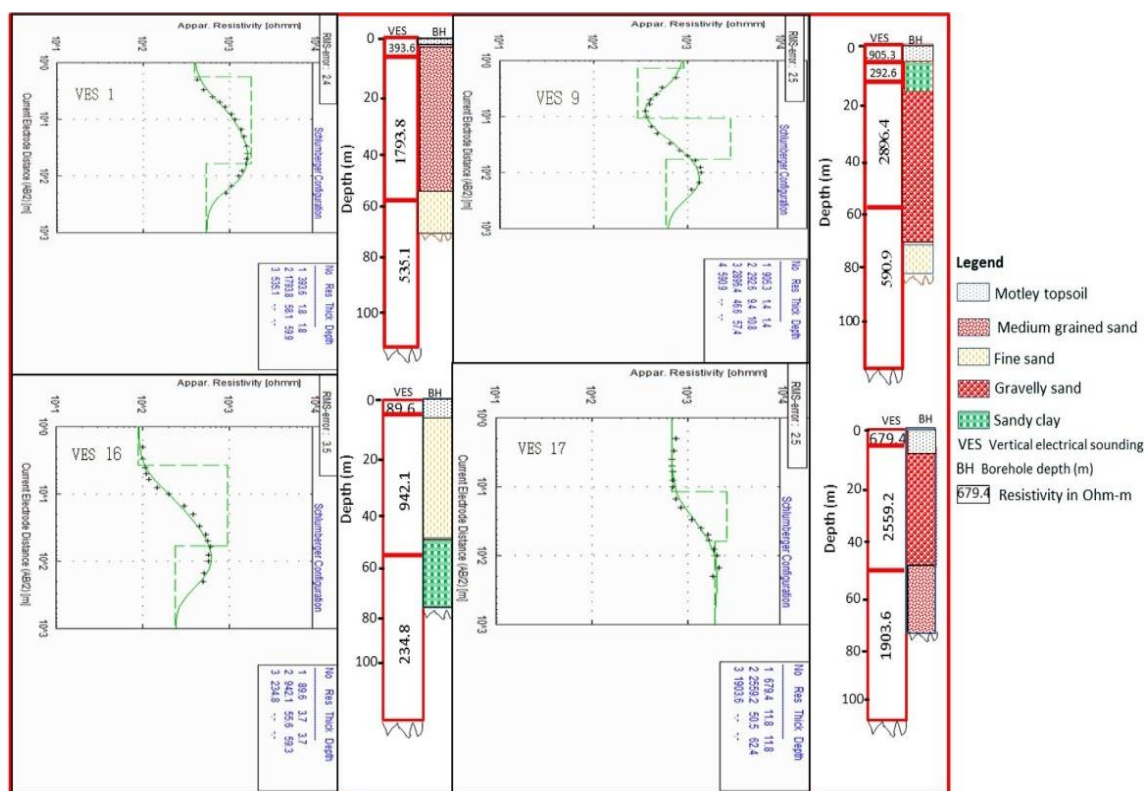


Fig. 3. Sampled correlations of VES 1, 9, 16 and 17 curves with their adjoining lithological log in the study area.

## 2 | Materials and Method

The research region employed the geo-sounding resistivity technology, which consisted of a 1-D Vertical Electrical Sounding (VES) and 2-D Electrical Resistivity Tomography (ERT). The IGIS signal enhancement resistivity meter SSP-MP-ATS and its accessories were used in close proximity to water wells for the execution of this technology. Twenty VES stations and ten ERT stations were selected based on the existing infrastructure in the area (Fig. 2). The VES process utilized the Schlumberger array, with a maximum spread (AB) of 400 m for the current electrodes. On the other hand, the 2-D technique employed the Wenner electrode configuration, with a spread length of 105 m, taken at 5 m intervals or separations [37]. Earth apparent resistance,  $R_{as}$  and  $R_{aw}$ , were measured in each VES and ERT technique, following the recommended precautions outlined by Zohdy et al. [18] and Akpan et al. [36]. The apparent resistivities  $\rho_{as}$  and  $\rho_{aw}$  for VES and ERT methods were determined using the equations provided in Eqs. (1) and (2), respectively.

$$\rho_{as} = n \cdot \frac{(AB/2)^2 - (MN/2)^2}{MN} \cdot R_{as} \tag{1}$$

$$\rho_{aw} = 2JraRaw, \tag{2}$$

where AB, MN and are, respectively, current electrode separation, potential electrode separation and Wenner electrode separations. The entire term multiplied by  $R_{as}$  and  $R_{aw}$  in Schlumberger and Wenner electrode configurations, respectively, to obtain the apparent resistivities  $\rho_{as}$ .

The apparent resistivities were graphed manually on a logarithmic scale using half of the current electrode separations. This was done to eliminate any noisy data points (outliers) that deviate from the overall trend of the curve. Subsequently, the curves were analyzed using a computer program called WINRESIST, which utilizes 1-D least square computer-assisted forward modelling. This software, developed by Vander Velpen and Sporry [38] in 1993, quantitatively interprets the data electronically. The analysis takes into account the

restrictions provided by adjacent logged borehole information. The software program provided data on the interpreted curve by determining the main geo-electric parameters such as layer resistivity, thickness, and depth. It also calculated the root-mean-square (usually less than 10%), which measures the accuracy of the fit between the theoretical curve and the actual field data (refer to Fig. 2). The ERT images were modelled by inverting the apparent resistivities obtained from Eq. (2). This was done by preparing the separation and apparent resistivity values together with the RES2DINV VER 3.59 Geotomo software code, which was developed by Loke and Barker [39], Loke and Dalhin [40], and Loke et al. [41]. The program constructs a resistivity model of the shallow subsurface using an iterative smoothness-constrained least squares method, as seen in the resulting ERT (Fig. 4). Table 1 presents the geographic information, as well as the measured and predicted hydrokinetic parameters of the shallowest aquifer that lies above the other deeper aquifers in the unconfined aquifer system.

## 2.1 | Porosity, Specific Yield and Specific Retention Estimations through Geoelectrical Resistivity Technology

The estimation of porosity, which measures the ability of a geological formation to hold water, was initiated by measuring the electrical conductivity of water  $\sigma_w = \frac{1}{\rho_w}$  in micro-Siemens per centimeter ( $\mu\text{Scm}^{-1}$ ) using a Combo EC and pH meter. The measured aw was transformed into water electrical resistivity  $\rho_w$  in Ohm-metre ( $\Omega\text{m}$ ) using the equation provided in Eq. (3).

$$\rho_w = \frac{c}{\sigma_w}. \quad (3)$$

The conversion factor from micro-Siemens per centimeter ( $\mu\text{Scm}^{-1}$ ) to Siemens per meter ( $\text{Sm}^{-1}$ ) is 104. Eq. (4) was used to estimate the total porosity of clean sand material in the saturated geologic block under consideration.

$$\phi = \left( \frac{a}{F} \right)^{\frac{1}{m}}. \quad (4)$$

The equation  $F = \frac{\rho_b}{\rho_w}$  represents the relationship between the formation factor and the bulk resistivity ( $\rho_b$ ).

The hydrogeological unit being discussed consists of geological formations with a coefficient of void space (also known as the coefficient of saturation). The average coefficient of the degree of cementation of the grain creating the porous medium is represented by the symbol  $m$ . The mean coefficients for  $a$  and  $m$  utilized in this investigation were determined in the study area by George et al. [10] as 0.5245 and 0.5, respectively.

The specific yield was determined by applying VES Geoelectrical Technology (GT) to the measured geoelectrical resistivity data. The formula used for this determination was based on the work of Tizro et al. [4] and Frohlich and Kelly [42]. The specific yield obtained from this method was found to be comparable to the specific yield obtained from Pumping Tests (PT) conducted by Tizro et al. [4] on similar geological formations. Eq. (5) was used for this determination.

$$s_y = \left( \frac{\rho_w}{\rho_{\text{sat}}} \right)^{\frac{1}{m}} \times \left[ 1 - \left( \frac{\rho_{\text{sat}}}{\rho_{\text{unsat}}} \right)^{\frac{1}{n}} \right]. \quad (5)$$

The resistivity of the saturated component of the aquifer, denoted as  $\rho_{\text{sat}}$ , is determined by subtracting the water resistivity ( $\rho_w$ ) obtained from the water conductivity (aw) from the bulk resistivity ( $\rho_b$ ) of the aquifer being studied.  $\rho_{\text{unsat}}$  refers to the resistivity of the unsaturated geological layer that sits above the uppermost aquifer in the unconfined aquifer system. The parameter  $m$  represents the coefficient that describes the extent of cemented grain formation in porous media. Similarly, the parameter  $n$  is also a coefficient, typically equal to 2 in most circumstances, similar to  $m$  [4]. This approach assumes that the soil/rock matrix (medium) acts

as an insulator, allowing electrical current to flow through it when water is in the pores [3], [20], [43], [44]. Samouëlian et al. [45] state that Geoelectrical Resistivity Technology (GRT) is a non-invasive method that provides continuous data over a sustainable duration at various spatial scales, from field to macroscopic scales, utilizing different electrode spacing configurations. According to Onu [46] and Tizro et al. [4], comparing GRT with PT reveals that GRT has lower labour and financial costs. This led to the decision to use GRT in this study to hydrodynamically analyze the shallow hydrogeological units in a medium-sized housing estate. Considering that electrical resistivity can be influenced by several factors related to the vertical and horizontal variations in geological properties, the existing borehole data in the study region were utilized to limit the interpretation and provide electrical resistivity data that is very accurate.

The specific retention, otherwise known as the field capacity ( $\phi_f$ ), is the difference between the total porosity ( $\phi$ ) and the gravity water porosity or specific yield  $s_y$  expressed as ( $\phi - \phi_f$ )

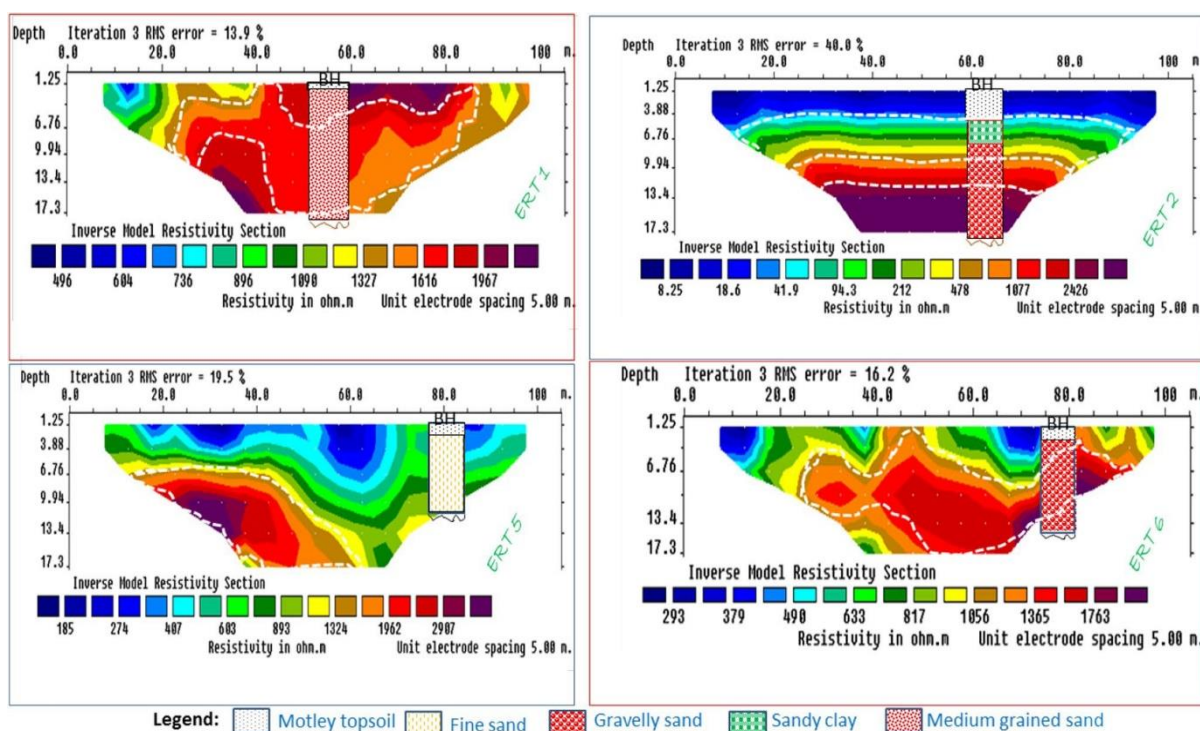


Fig. 4. Representatives of ERTs 1, 2, 5 and 6 with their adjoining lithological log in the study area.

Tortuosity, also known as a tortuous flow route, is an inherent characteristic of a porous medium. It is defined as the ratio of the actual length of the flow path to the straight distance. Tortuosity is commonly used to characterize porous geological media's diffusion and fluid movement. The situation calculated using Eq. (6).

$$\gamma = \sqrt{F\phi}. \quad (6)$$

## 2.2 | Hydraulic Conductivity and Permeability of the Topmost Medium of the Unconfined Aquifer

The hydraulic conductivities ( $k_h$ ) were quantitatively determined using the Kozeny-Carman-Bear's equation, based on the total porosity ( $\phi$ ) and site mean diameter ( $d_m$ ) values obtained from measurements ranging from 0.00035-0.00097 m using a digital micrometre screw gauge.

$$k_h = \left( \frac{\delta_w \cdot g}{\mu_d} \right) \cdot \left( \frac{d_m^2}{180} \right) \cdot \left( \frac{\phi^3}{(1-\phi)^2} \right). \quad (7)$$

**Table 1. Measured and estimated hydrokinetic properties associated with the aquifer system**

VES/ERT No	Location	Long. (Deg.)	Lat. (Deg.)	Aw(S/M)	Pw	Pb	Psat	F	Punsat	ϕ
1/1	Imoh ita	7.9492	4.9791	0.000711	1406.9	1793.8	386.9	1.27	393.6	0.641
2	Murray avenue	7.9522	4.9790	0.000587	1702.9	2051.9	349.0	1.20	351.8	0.660
3/2	Ambasador ubok udom	7.9506	4.9778	0.00496	201.6	779.9	578.3	3.87	1234.4	0.368
4/3	Kufre ekanem Crescent	7.9517	4.9750	0.00061	1639.6	2591.8	952.2	1.58	996.3	0.576
5/4	Godswill akpabio Crescent 4	7.9594	4.9745	0.009434	106.0	411.9	305.9	3.89	1464.2	0.367
6	Udo udoma street	7.9606	4.9786	0.00052	1923.0	2109.9	186.9	1.10	187.6	0.691
7	Alison attah	7.9619	4.9815	0.010989	91.0	301.1	210.1	3.31	560.5	0.398
8/7	Godswill akpabio Crescent 1	7.9531	4.9800	0.009174	109.0	427.1	318.1	3.92	1121.1	0.366
9	Godswill akpabio Crescent 2	7.9556	4.9862	0.013699	73.0	292.6	219.6	4.01	905.3	0.362
10	Godswill akpabio Crescent 3	7.9597	4.9878	0.059524	16.8	71.2	54.4	4.24	361.1	0.352
11/10	Shelter afrique entrance	7.9614	4.9855	0.001617	618.3	1131.4	513.1	1.83	562.2	0.535
12/8	Chris ekpenyong	7.9639	4.9830	0.000558	1793.4	2085.8	292.4	1.16	294.2	0.672
13	Sunday Mbang street	7.9644	4.9820	0.052356	19.1	81.0	61.9	4.24	348.3	0.352
14	Aniekan Umana street	7.9658	4.9835	0.071429	14.0	53.0	39.0	3.79	110.5	0.372
15/9	Godswill akpabio Crescent 5	7.9675	4.9838	0.1	10.0	43.7	33.7	4.37	208.3	0.346
16	Akpan hogan ekpo avenue	7.9550	4.9878	0.001172	852.9	942.1	89.2	1.10	89.6	0.689
17	Justice edet robert	7.9539	4.9877	0.000526	1900.0	2559.2	659.2	1.35	679.4	0.624
18/5	Engr atayu Ekwerre	7.9525	4.9867	0.000956	1045.9	1255.5	209.6	1.20	211.8	0.661
19/6	Dan udofia avenue	7.9522	4.9853	0.000662	1510.0	1938.8	428.8	1.28	436.5	0.639
20	Uduak udoudoh avenue	7.9494	4.9755	0.021322	46.9	308.3	261.4	6.57	1409.0	0.282
Mean	0.144	754.0	81,918.1	307.5	2.38	596.3	0.470	0.075	0.395	21.4
Range	0.004–0.6218	10.0–1923.0	43.7–2591.8	0.282–0.691	0.040–0.107	0.242–0.623	57.4–4339.2	91.7–7269.7	5.0–77.7	

VES/ERT No	Location	Long. (Deg.)	Lat. (Deg.)	s <sub>y</sub>	ϕ <sub>f</sub>	kh	kp	h
1/1	Imoh ita	7.9492	4.9791	0.063	58.1	58.1	58.1	58.1
2	Murray avenue	7.9522	4.9790	0.046	52.6	52.6	52.6	52.6
3/2	Ambasador ubok udom	7.9506	4.9778	0.062	7.8	7.8	7.8	7.8
4/3	Kufre ekanem Crescent	7.9517	4.9750	0.052	23.4	23.4	23.4	23.4
5/4	Godswill akpabio Crescent 4	7.9594	4.9745	0.106	19.3	19.3	19.3	19.3
6	Udo udoma street	7.9606	4.9786	0.058	72.4	72.4	72.4	72.4
7	Alison attah	7.9619	4.9815	0.107	16.6	16.6	16.6	16.6
8/7	Godswill akpabio Crescent 1	7.9531	4.9800	0.090	15.0	15.0	15.0	15.0
9	Godswill akpabio Crescent 2	7.9556	4.9862	0.093	9.4	9.4	9.4	9.4
10	Godswill akpabio Crescent 3	7.9597	4.9878	0.100	29.5	29.5	29.5	29.5
11/10	Shelter afrique entrance	7.9614	4.9855	0.060	69.9	69.9	69.9	69.9
12/8	Chris ekpenyong	7.9639	4.9830	0.050	50.2	50.2	50.2	50.2
13	Sunday Mbang street	7.9644	4.9820	0.094	5.6	5.6	5.6	5.6
14	Aniekan Umana street	7.9658	4.9835	0.084	18.3	18.3	18.3	18.3
15/9	Godswill akpabio Crescent 5	7.9675	4.9838	0.092	77.7	77.7	77.7	77.7
16	Akpan hogan ekpo avenue	7.9550	4.9878	0.073	55.6	55.6	55.6	55.6
17	Justice edet robert	7.9539	4.9877	0.077	50.5	50.5	50.5	50.5
18/5	Engr atayu Ekwerre	7.9525	4.9867	0.062	73.0	73.0	73.0	73.0
19/6	Dan udofia avenue	7.9522	4.9853	0.062	56.1	56.1	56.1	56.1
20	Uduak udoudoh avenue	7.9494	4.9755	0.040	5.0	5.0	5.0	5.0
Mean range	0.144	754.0	81,918.1	2445.2	38.3			
	0.004–0.6218	10.0–1923.0	43.7–2591.8	s <sub>y</sub>	ϕ <sub>f</sub>			
	33.7–952.2	1.1- 6.57	89.6–1464.2					

aw: water electrical conductivity (S/m), pw: water resistivity (Ω m), F: formation factor, kp: permeability (mD), kh: hydraulic conductivity (m/day), pb: bulk resistivity of the topmost aquifer (Ω m), psat: resistivity of saturated part of aquifer (Ω m), punsat: resistivity of unsaturated part of aquifer (Ω m), Sy: Specific yield, ϕ<sub>f</sub>: specific retention and h: thickness (m) of shallowest aquifer considered.

The density of water,  $\delta_w$ , is 1000 kg/m<sup>3</sup>. The dynamic viscosity of water,  $\mu_d$ , is approximately 0.0014 kg/m s, according to Fetters [47]. The acceleration due to gravity, g, is taken as 9.8 m/s<sup>2</sup>. The permeability (kp) of the uppermost aquifer was determined using the water density ( $\delta_w$ ), hydraulic conductivity (Kh), water dynamic viscosity ( $\mu_d$ ), and gravitational acceleration, as described by Eq. (8).

$$K_p = K_h \cdot \mu_d / \delta_w \cdot g \quad (8)$$

The estimated values of kp in m<sup>2</sup> were converted to millidarcy (mD) by multiplying the values in m<sup>2</sup> by a conversion factor of  $1.01325 \times 10^{12}$  according to George [20].



## 2.3 | Protectivity and Potentiality of Shallow Unconfined Hydrogeological Units Assessed

The protective capacity and potential of the unconfined/open aquifers in the medium-sized housing estate in Shelter Afrique were assessed using the Dar Zarrouk parameters. The longitudinal conductance (S) was estimated as  $h/p$  in Siemens, while the Transverse Resistance (TR) was expressed as  $(h \cdot p)$  in  $\Omega m^2$ . Additionally, the Transmissivity (T) was estimated as  $(k \cdot h)$  in  $m^2 s^{-1}$ . Protecting an aquifer system relies on the characteristics of the lithological unit that covers and surrounds it. The level of protection and susceptibility to surface contamination is directly related to its longitudinal conductance S. Longitudinal conductance values below 1.0 Siemens suggest that the overburden medium has a negligible amount of impermeable argillites above the aquifer system, indicating a high rate of infiltration for surface contaminants.

## 3 | Result and Discussion

The GRT was corroborated by mechanical boreholes adjacent to the profiles, aiding in the interpretation of VES and ERT data. The primary objective of electrical studies is to accurately determine the subsurface resistivity distribution by conducting measurements on either the surface or a borehole [48]. An electrical current is applied to the ground using a set of current electrodes, and the resulting voltage is measured using another set of electrodes. The variability in resistivity was determined by performing inversion, which involves finding the resistivity model that best fits the whole sequence of quadrupole observations. The apparent resistivities were calculated using *Eqs. (1) and (2)* [49]. The nonlinear problem of inversion was numerically solved using iterative techniques, as described by Tripp et al. [50] in 1984. In order to avoid any confusion, the actual resistivities were taken into account when discussing the matter.

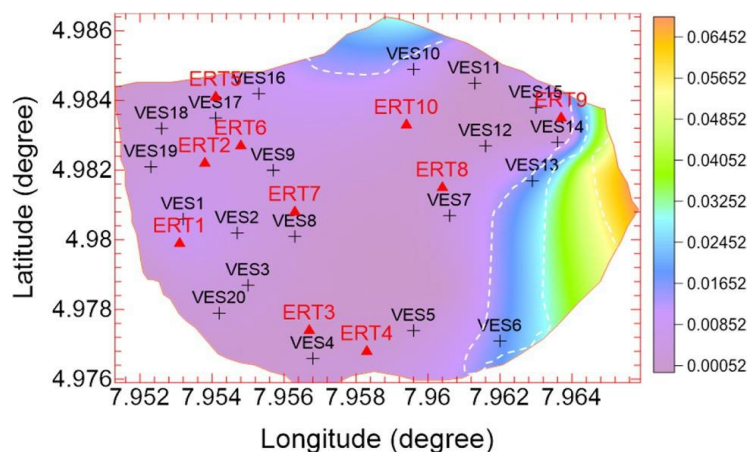
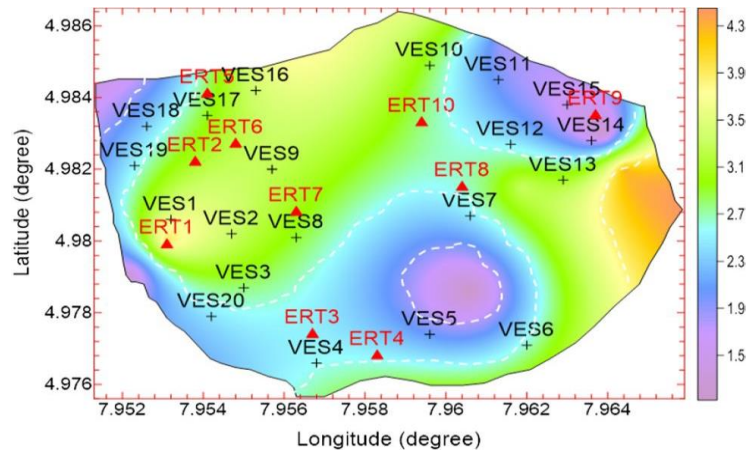


Fig. 5. 2-D image map of the distribution of water conductivity (microSiemens per centimetre) in the study area.



**Fig. 6. 2-D image map of the distribution of formation factor in the topmost aquifer in the study area.**

Adjacent mechanical boreholes corroborated the GRT data interpretation from VES and ERT. The primary objective of electrical investigations is to accurately determine the subsurface resistivity distribution cost-effectively, using measurements taken either on the surface or in a borehole [48]. An electrical current is applied to the ground using a set of current electrodes, and the resulting voltage is measured using another set of electrodes. The variability of resistivity was assessed by performing inversion, which involves determining the resistivity model that best matches the whole sequence of quadrupole observations. The apparent resistivities were calculated using *Eqs. (1) and (2)* [49]. Using iterative techniques, numerical methods were employed to solve the nonlinear inversion problem [50]. In order to avoid any confusion, the actual resistivities were considered when discussing the unknown situation. The term computed resistivities refers to resistivities obtained using inversion. The term apparent resistivities encompasses both real and computed resistivities derived from direct voltage measurements conducted in assumed homogenous mediums.

The issues of VES and ERT, considered inverse problems, are characterized as ill-posed or ill-constrained, meaning that their solutions can be unstable or non-unique. This study's VES and ERT interpretations were limited by adjacent mechanical boreholes close to their measurement locations (refer to *Figs. 3 and 4*). The findings indicate that the subsurface through which the current flowed can be characterized by both high and low resistivities/conductivities. This is shown in the 2-D map of conductivity in *Fig. 5*. The ERT visually represents the geological pattern and trend in the shallowest layers.

On the other hand, the VES of the GRT provides curves that describe the electrical characteristics of the soil matrix and its pore occupants. These characteristics are also associated with changes in the hydro-hydraulic facies. The electrode separations successfully penetrated a maximum of three to four subsurface layers. The resistivity of the first layer varied between 89.6 and 1464.2  $\Omega\text{m}$ , with an average value of 596.3  $\Omega\text{m}$ . The thickness of this stratum varied between 1.2 and 11.8 meters, with an average value of 4 meters. Layer 1 is not fully saturated and is connected to the water table, which is the upper boundary of layer 2. The second layer has a bulk resistivity range of 43.7–2591.8  $\Omega\text{m}$ , with a mean value of 1793.8  $\Omega\text{m}$ . This layer has a thickness range of 5.0 to 77.7 meters, with an average thickness of 38.3 meters. Layers three and four, located below layer two (the shallowest aquifer in the research area), are penetrated by current at its maximum current electrode separation. The resistivity values for layers 3 and 4 ranged from 220 to 2896.4  $\Omega\text{m}$ , with a mean value of 1244.7  $\Omega\text{m}$  for layer 3 and 206.7 to 1194.6  $\Omega\text{m}$ , with a mean value of 634.8  $\Omega\text{m}$  for layer 4. As the thickness of layer four was unspecified, layer three only has a thickness that varies between 41.7 and 58.1 meters, with an average thickness of 49.8 meters.

Regarding the saturated units, the conductivity, as demonstrated by the picture map, diminishes from the eastern region to the western region. The picture map in *Fig. 6* illustrates the spatial distribution of the formation factor, which is influenced by the characteristics of the pore-fluid and lithological textures, as Ekanem et al. [51] suggested. The arrangement of the colour codes on the map reflects the diversity of the

formation factor at different VES and ERT locations. Based on the data presented in Fig. 6, it can be observed that VESs 4, 5, 6, 7, 11, 12, 14, 15, 18, and 19, along with their related ERTs, have low values. The decrease in formation factor substantially impacts the increase of the overall porosity in the aquifer system. The resistivity distributions shown in Figs. 7.a-7.d reveal a clear correlation between the resistivity of the unsaturated part of the aquifer (punsat) and the resistivity of the saturated part of the aquifer (psat), as well as between the bulk resistivity of the topmost aquifer (pb) and the resistivity of the water (pw). The observed pattern in the resistivity distributions suggests that water impacts the resistivity of geological units. The resistivity distribution on the image map demonstrates the ability to identify patterns within the surface and subsurface soil matrices. It serves as a quantification of the selected route through which electrical current flows in the geological units. It is important to note that current prefers to flow through areas with low resistivity, indicating the presence of fluid that may be temporarily or permanently trapped in the pores of the soil or rock.

The total porosity of a material is determined by the combination of its gravity water porosity (also known as specific yield) and specific retention (also known as field capacity). This porosity is influenced by factors such as the arrangement of grain sizes, the geometry of the material, the extent of voids, and the interconnection of the intrinsic pores through which water accumulates [9]. Mazáč et al. [11] found that grain size does not impact total porosity in sediments with homogeneous sizes. Instead, the arrangement of the grains solely influences porosity, which can decrease as particle size increases.

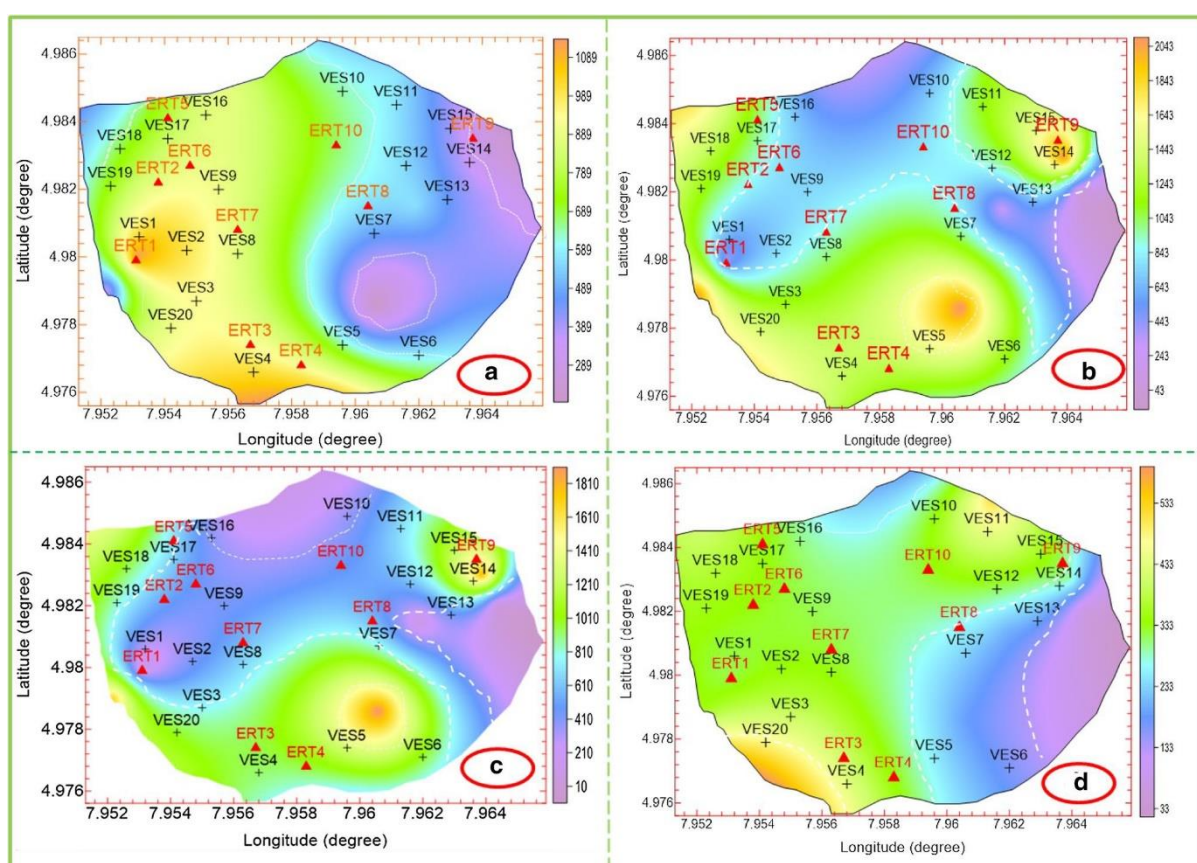


**Fig. 7. 2-D image map of the distribution of a. resistivity of unsaturated part of aquifer punsat, b. topmost aquifer bulk resistivity pb, c. water resistivity pw, and d. topmost resistivity of saturated part of aquifer psat in the study area.**

However, the measurements of grain size diameters (ranging from 0.00035 to 0.00097 m with a mean of 0.00061 m) indicate that the aquifer system consists of sediments that vary in size from fine to medium and medium to coarse-grained sands (as shown in Table 2). These sediments can be described as intercalated non-uniform grain size, a notable characteristic of the Benin Formation [37], [52] in the study area. The figures in Fig. 8 demonstrate the relationship between the hydrokinetic properties and the lithological units in the



unconstrained aquifers of the medium-sized housing estate. These figures include total porosity, specific yield, specific retention (or field capacity), and tortuous flow path. Fig. 8.a shows a significant association between total porosity and specific retention or field capacity, as shown in Fig. 8.c. This finding is consistent with the research conducted by Karanath [9] in 1994. This relationship can be attributed to the distinct properties of retained water in some pores throughout the aquifer system [13]. The picture maps depicting the specific field (Fig. 8.b) and tortuosity (Fig. 8.d) exhibit a substantial correlation. Conversely, the images in Figs. 8.a and 8.c display an inverted recognition pattern compared to Figs. 8.b and 8.d.

Consequently, VES points (5, 6, 7, 11, 14, 15, and 18) and their accompanying ERT, linked to less complex flow paths, will have lower specific yield. As a result, they will have better field capacity or specific retention, as stated by Ekanem [53] in 2020. VES points with low specific yield but high specific retention will likely retain a larger portion of water due to capillary forces and adhesion when the hydrogeological unit is drained. As a result, aquifers located below the topmost aquifer in the open aquifer system at these locations may be more suitable for groundwater extraction.

**Table 2. Ranges of the diameter of soil particle sizes [54].**

Soil Particle	Diameter (dm)(mm)	Diameter (dm)(m)
Very coarse sand	2.00–1.00	0.002–0.001
Coarse sand	1.00–0.50	0.001–0.0005
Medium sand	0.50–0.25	0.0005–0.00025
Fine sand	0.25–0.10	0.00025–0.0001
Very fine sand	0.10–0.05	0.0001–0.00005
Silt	0.05–0.002	0.00005–0.000002
Clay	< 0.002	< 0.000002

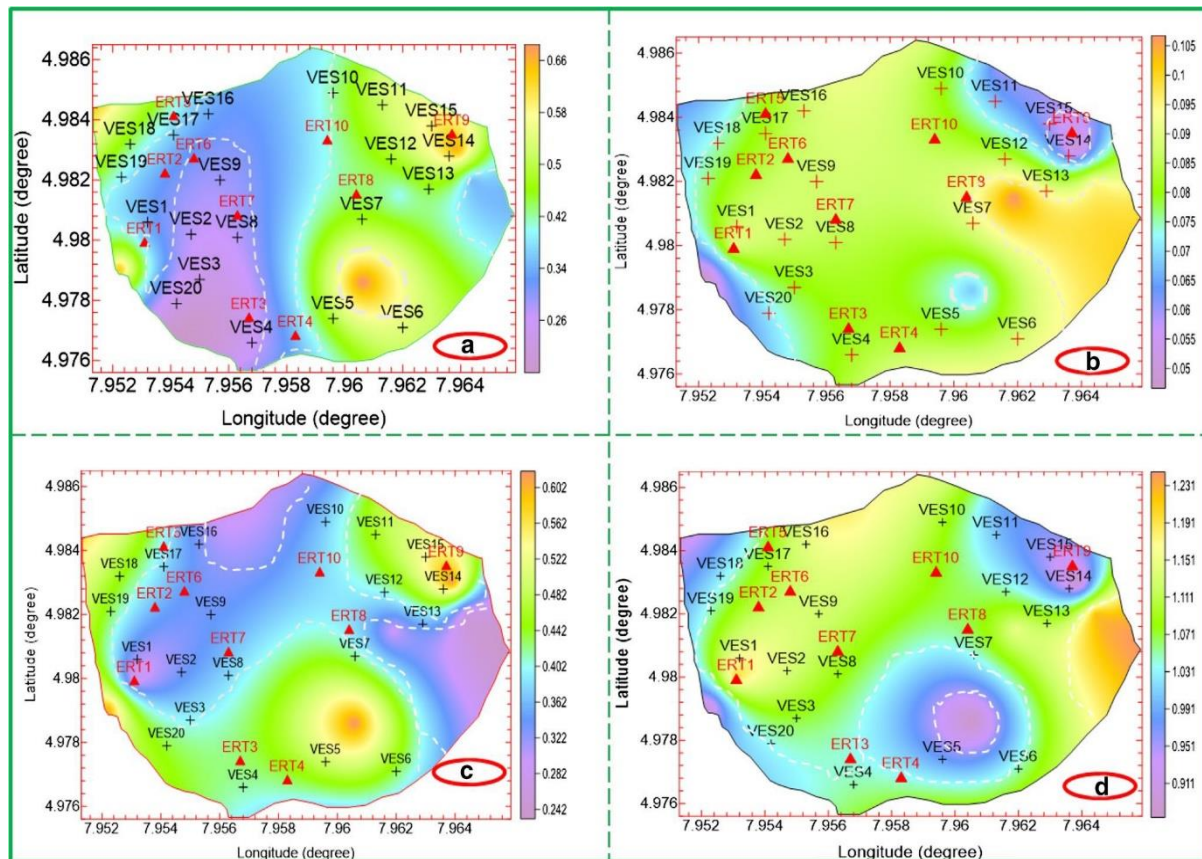


**Fig. 8. 2-D Image map of the distribution; a. topmost aquifer total porosity, b. topmost aquifer gravity water porosity or specific yield, c. topmost aquifer specific retention or field capacity, and d. topmost aquifer tortuosity in the study area.**



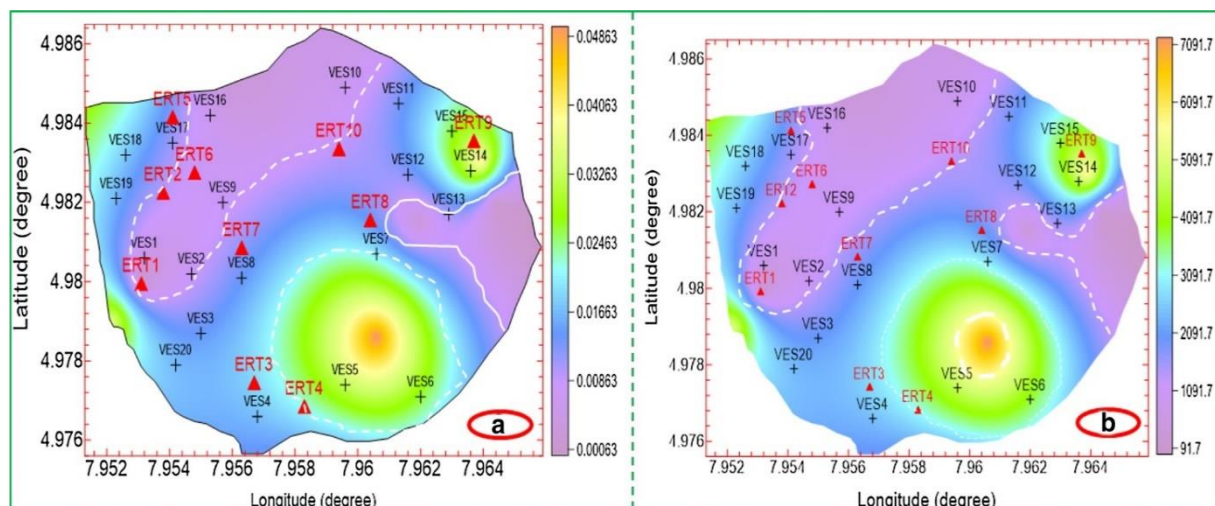


**Fig. 9. 2-D image map of the distribution; a. topmost aquifer hydraulic conductivity (m/s), and b. topmost aquifer permeability (mD) in the study area.**

Fig. 9 displays the hydraulic conductivity (measured in meters per second) and permeability (measured in millidarcies) of the uppermost aquifer in the open aquifer system. The picture maps for the two hydrodynamical parameters exhibit comparable patterns, with distinct categories of low, moderate, and high values for hydraulic conductivity and permeability, respectively. The study by Vázquez-Báez et al. [55] found that areas with high permeability and hydraulic conductivity allow fluid to be transmitted easily. In contrast, areas with intermediate and low values imply a slower rate of fluid transmission within the aquifer system in the study area. The region containing VESs 5, 6, 14, and 15, along with their related ERTs, exhibit a relatively high permeability and hydraulic conductivity, as shown in Fig. 9.

TR is a geo-electric measure that quantifies the degree of groundwater potential. It is directly related to T, the speed at which water flows through a specific width of aquifer under a specific hydraulic gradient. Gheorghe [56] considered T to be an indicator of aquifer potential. According to Obiora et al. [25], a high TR indicates strong T values and a high potential for the hydrogeological unit, as seen in Tables 3 and 4. Fig. 10 displays the image map for T and TR in parts a and b. The maps display a consistent pattern with colour codes indicating areas with low values (at VESs: 1, 2, 3, 8, 12, 13, and 16), moderate values (at VESs: 3, 4, 7, 8, 10, 15, 18, and 20), and high values (at VESs: 5, 6, and 14), along with their corresponding ERTs. The patterns observed in the images of T (a) and TR (b) closely resemble the patterns observed in the hydraulic conductivity (a) and permeability (b) of Fig. 9. It indicates that these characteristics are directly proportional to each other. Those with moderate and high permeability values exhibit favourable groundwater potential, whereas those with comparatively low values offer moderate groundwater potential within the unconfined aquifer system. Nevertheless, there are concerns about the overall effectiveness of the aquifer system in protecting against contamination due to its relatively low longitudinal conductance, which ranges from 0.004 to 0.6218 Siemens (Table 5). The numbers indicate a level of protection that ranges from low to moderate [26], [57] (Fig. 10.c).

**Table 3. T/aquifer potential scale [56].**

Range	Potential
> 500m <sup>2</sup> /day	High
50–500 m <sup>2</sup> /day	Moderate
5–50 m <sup>2</sup> /day	Low
0.5–5 m <sup>2</sup> /day	Very low
< 0.5 m <sup>2</sup> /day	Negligible

The image map of Fig. 10.c, representing longitudinal conductance, exhibits a comparable pattern recognition as observed in Fig. 10.a, representing aquifer T. This might be attributed to the correlation between the reliability of these two factors and the thickness of the aquifer being considered in the aquifer system. The

picture map of Storage-dependent Drainable Efficiency (SDE), expressed as  $\left(\alpha = \frac{s_y}{\phi} \times 100\right)$  in Fig. 10(d),

exhibits a completely reversed order compared to the distribution of T, TR, and longitudinal conductance. The parameters T and TR drop exponentially, as illustrated in Fig. 11, using Eqs. (9) and (10), respectively.

$$T = 1 \times 108a - 3.047. \quad (9)$$

$$TR = 4 \times 10^7 a^{-2.74}. \quad (10)$$

The abovementioned equations exhibit a high coefficient of determination, specifically 0.6 and 0.7 for T and TR, respectively. This demonstrates a strong link. The specific yield is the proportion of the volume fraction that can be easily released compared to the fraction that remains trapped in the drainable pore during groundwater pumping. The values observed in the unconfined aquifer system examined varied between 7.6% and 40.5%, averaging 21.4%. The magnitude of the increase is directly proportional to the rise in specific yield and inversely proportional to the increase in specific retention (Fig. 11). In order to get the best possible discharge of water from the drainable pores into wells for pumping, it is necessary to surpass the junction point of specific yield and specific retention as shown in Eqs. (11) and (12) in Fig. 11.

$$\phi f = -0.0116a + 0.6714. \quad (11)$$

$$s_y = 0.0015a + 0.0423. \quad (12)$$

Based on the study, it is probable that an SDE value exceeding 21% is both realistic and optimal for sustainable groundwater extraction in the medium-sized housing estate. Fig. 10(d) shows the distribution of values. The area is slightly inefficient in terms of releasing pore water into wells for pumping since areas with less than 21% make up a tiny percentage in the northeast (VESs: 11, 14, and 15), northwest (VESs: 18 and 19), southwest (VES: 20), and southeast (VES: 5). The remaining portion of the plotted area has a percentage greater than 21%. Nevertheless, as the longitudinal conductance map indicates, the region is highly susceptible to contamination because of its fragile protective layer. The innovative aspect of this work, as demonstrated in Fig. 12, lies in identifying and utilizing specific yield and field capacity for groundwater exploration. This is achieved by applying surface geophysics, leading to the subsequent exploitation of groundwater resources. This surpasses the typical calculation of specific yield and field capacity, as Todd [16] suggested, determining the amount of water stored in an aquifer. This is because they are further aggregated here to calculate the most and least suitable areas for the groundwater available for extraction.

**Table 4. Geophysical and hydraulic parameters of various locations.**

VES Number	ERT Number	Location	Transverse Resistance ( $\Omega m^2$ )	Longitudinal Conductance S (mhos)	ASPC Rating	Transmissivity ( $m^2/day$ )	Comparative Aquifer Potentials
1	1	Imoh ita	104,219.78	0.148	Weak	149,033.1	Very high
2		Murray avenue	107,929.94	0.150	weak	163,159.5	Very high
3	2	Ambasador ubok	6083.22	0.006	Poor	1219.7	High
4	3	Udom					
		Kufre ekanem	60,648.12	0.023	Poor	31,108.0	Very high
5	4	Crescent					
		Godswill akpabio	7949.67	0.013	Poor	2990.0	High
6		Crescent 4					
		Udo udoma street	152,756.76	0.386	Moderate	314,158.9	Very high
7		Alison attah	4998.26	0.030	Poor	3616.0	High
8	7	Godswill akpabio	6406.5	0.013	Weak	2284.0	High
9		Crescent 1					
		Godswill akpabio	2750.44	0.010	Poor	1365.6	High
10		Crescent 2					
		Godswill akpabio	2100.4	0.082	Poor	3821.7	High
		Crescent 3					

Table 4. Continued.

VES Number	ERT Number	Location	Transverse Resistance R ( $\Omega\text{m}^2$ )	Longitudinal Conductance S (mhos)	ASPC Rating	Transmissivity ( $\text{m}^2/\text{day}$ )	Comparative Aquifer Potentials
11	10	Shelter afrique entrance	79,084.86	0.124	Weak	62,123.7	Very high
12	8	Chris ekpenyong	104,707.16	0.171	Weak	176,187.6	Very high
13		Sunday mbang street	453.6	0.016	Poor	724.5	Moderate
14		Aniekan umana street	969.9	0.166	Weak	2993.9	High
15	9	Godswill akpabio Crescent 5	3395.49	0.373	Moderate	9456.9	High
16		Akpan hogan ekpo avenue	52,380.76	0.621	Moderate	235,294.9	Very high
17		Justice edet robert	129,239.6	0.074	Poor	108,529.9	Very high
18	5	Engr atauyo ekwerre	91,651.5	0.345	Moderate	229,394.0	Very high
19	6	Dan udofia avenue	108,766.68	0.129	Weak	140,625.4	Very high
20		Uduak udoudoh avenue	1541.5	0.004	Poor	273.7	Low
Mean				0.144		81,918.1	
51,401.7							
Range				0.004–0.6218		273.7–314,158.9	
453.6–							
152,756.5							

## 4 | Conclusion

The GRT and geological information have been used to map the shallowest hydrogeological unit of the unconfined aquifer system in a medium-sized housing estate of Shelter Afrique. The findings unveiled the dispersion of several characteristics and the ability to safeguard the potential of the aquifer system in the highly sought-after residential area in Akwa Ibom State, Southern Nigeria. The findings indicated that the hydrogeological units, consisting of fine- to medium- and medium- to coarse-grained sands, have a high capacity for extracting groundwater. However, they offer only moderate to poor protection, as indicated by the T/aquifer potential Scale [56] and the range of values for longitudinal conductance that determine the protective scale [57].

**Table 5. Modified longitudinal unit conductance and its protective capacity rating [57].**

Longitudinal Conductance	Protective Capacity Rating
> 10.00	Excellent
5.00–10.00	Very good
0.70–4.90	Good
0.20–0.69	Moderate
0.10–0.19	Weak
< 0.10	Poor

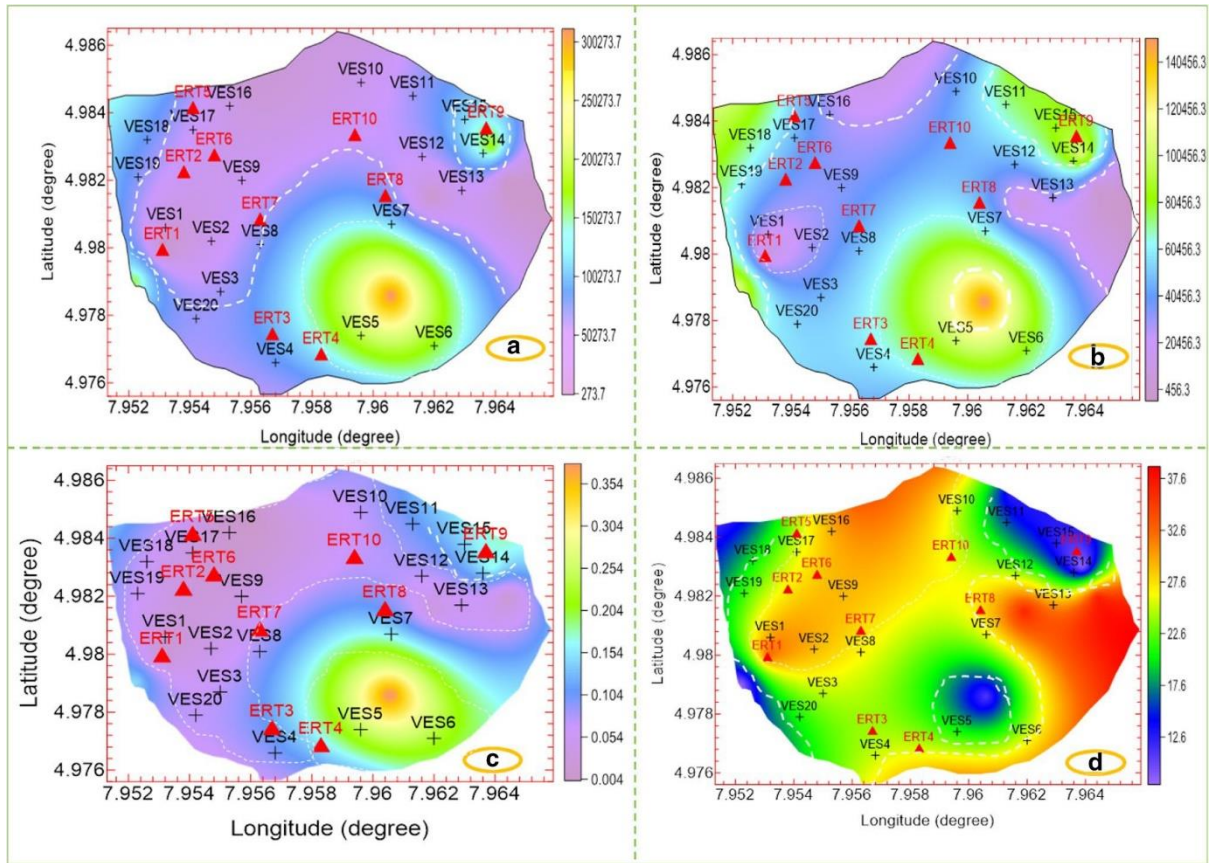


Fig. 10. 2-D image map of the distribution; a. topmost aquifer T (m<sup>2</sup>/day), b. topmost aquifer TR (Ω m<sup>2</sup>), c. top-most aquifer longitudinal conductance (Siemens), and d. storage-dependent drainability efficiency (%).

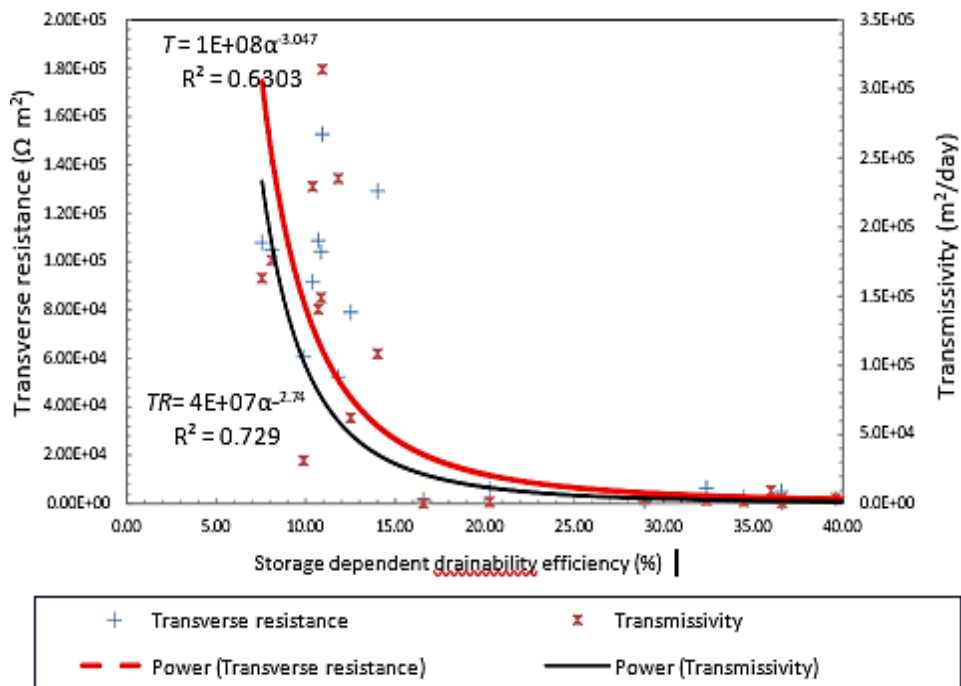


Fig. 11. A plot of transverse and transmissivity (m<sup>2</sup>/day) and transverse resistance (Ωm<sup>2</sup>) against SDE (%).



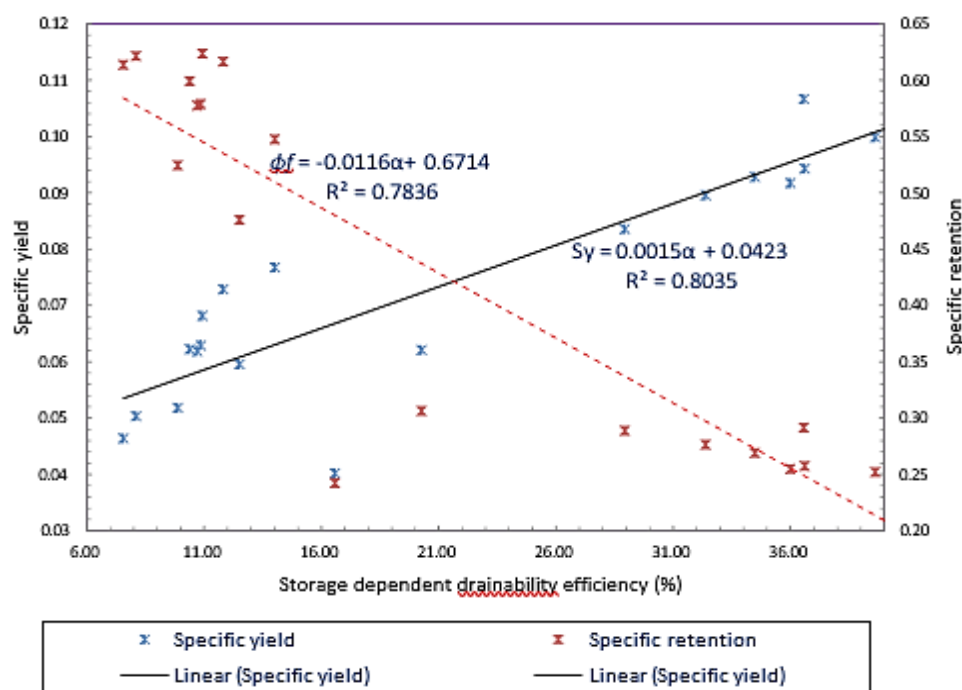


Fig. 12. Specific yield and specific retention against SDE (%).

The hydrokinetic parameters inferred from geological information align with those obtained from similar geological conditions both within and outside the study area. The innovative aspect of this study lies in the determination of the specific yield and field capacity, as well as the SDE, which provides a hydrodynamic explanation for the dynamics of pores and the factors that affect the optimal and effective extraction of pore water through well pumping. An analysis has been conducted to determine the aquifer system's hydrokinetic characteristics, parametric maps, and potential and protectivity maps. This analysis aims to facilitate the efficient extraction, monitoring, and management of groundwater resources. Given the high demand for living in this newly constructed housing estate, it is crucial to establish effective waste disposal systems to prevent the leakage and contamination of harmful substances such as leachates and other organic/inorganic waste into the underlying hydrogeological units. These units store groundwater extracted for various purposes and are naturally susceptible to damage.

## References

- [1] Niwas, S., & Singhal, D. C. (1985). Aquifer transmissivity of porous media from resistivity data. *Journal of hydrology*, 82(1–2), 143–153. <https://doi.org/10.1093/geront/30.1.43>
- [2] Bhatt, K. (1993). Uncertainty in wellhead protection area delineation due to uncertainty in aquifer parameter values. *Journal of hydrology*, 149(1–4), 1–8. [https://doi.org/10.1016/0022-1694\(93\)90095-Q](https://doi.org/10.1016/0022-1694(93)90095-Q)
- [3] Niwas, S., Tezkan, B., & Israil, M. (2011). Aquifer hydraulic conductivity estimation from surface geoelectrical measurements for Krauthausen test site, Germany. *Hydrogeology journal*, 19(2), 307–315. DOI: 10.1007/s10040-010-0689-7
- [4] Tizro, A. T., Voudouris, K., & Basami, Y. (2012). Estimation of porosity and specific yield by application of geoelectrical method--a case study in western Iran. *Journal of hydrology*, 454, 160–172. <https://doi.org/10.1016/j.jhydrol.2012.06.009>
- [5] Frind, E. O., & Molson, J. W. (2018). Issues and options in the delineation of well capture zones under uncertainty. *Groundwater*, 56(3), 366–376. <https://doi.org/10.1111/gwat.12644>
- [6] Hilberts, A. G. J., Troch, P. A., & Paniconi, C. (2005). Storage-dependent drainable porosity for complex hillslopes. *Water resources research*, 41(6). <https://doi.org/10.1029/2004WR003725>

- [7] George, N. J., Obianwu, V. I., & Obot, I. B. (2011). Laboratory estimation of aquifer effective porosities from core samples obtained during borehole drilling in parts of the Niger Delta Region, South-eastern Nigeria. *Advances in applied science research*, 2(1), 153–162.
- [8] Fetter, C. W. (1988). *Applied hydrogeology*. Waveland Press.
- [9] Karanath, K. R. (1994). *Hydrogeology*. Mc Graw-Hill Publishing.
- [10] George, N. J., Emah, J. B., & Ekong, U. N. (2015). Geohydrodynamic properties of hydrogeological units in parts of Niger Delta, Southern Nigeria. *Journal of african earth sciences*, 105, 55–63. <https://doi.org/10.1016/j.jafrearsci.2015.02.009>
- [11] Mazáč, O., Kelly, W. E., & Landa, I. (1985). A hydrogeophysical model for relations between electrical and hydraulic properties of aquifers. *Journal of hydrology*, 79(1–2), 1–19. [https://doi.org/10.1016/0022-1694\(85\)90178-7](https://doi.org/10.1016/0022-1694(85)90178-7)
- [12] Schwartz, F. W., & Zhang, H. (2024). *Fundamentals of groundwater*. John Wiley & Sons.
- [13] Dietrich, S., Carrera, J., Weinzettel, P., & Sierra, L. (2018). Estimation of specific yield and its variability by electrical resistivity tomography. *Water resources research*, 54(11), 8653–8673. [https://doi.org/10.1016/0022-1694\(85\)90178-7](https://doi.org/10.1016/0022-1694(85)90178-7)
- [14] Luo, Z., Shen, C., Kong, J., Hua, G., Gao, X., Zhao, Z., ... & Li, L. (2018). Effects of unsaturated flow on hillslope recession characteristics. *Water resources research*, 54(3), 2037–2056. <https://doi.org/10.1002/2017WR022257>
- [15] Nielsen, P., & Perrochet, P. (2000). Watertable dynamics under capillary fringes: experiments and modelling. *Advances in water resources*, 23(5), 503–515. [https://doi.org/10.1016/S0309-1708\(99\)00038-X](https://doi.org/10.1016/S0309-1708(99)00038-X)
- [16] Todd, D. K. (1980). *Ground water hydrology*. Wiley.
- [17] Hamill, L., & Bell, F. (1986). *Groundwater resources development*. Butterworths Publications.
- [18] Zohdy, A. A. R., Eaton, G. P., & Mabey, D. R. (1974). *Application of surface geophysics to ground-water investigations*. <https://pubs.usgs.gov/publication/twri02D1>
- [19] Zohdy, A. A. R. (1989). A new method for the automatic interpretation of Schlumberger and Wenner sounding curves. *Geophysics*, 54(2), 245–253. <https://doi.org/10.1190/1.1442648>
- [20] George, N. J. (2020). Appraisal of hydraulic flow units and factors of the dynamics and contamination of hydrogeological units in the littoral zones: a case study of Akwa Ibom State University and its Environs, Mkpato Enin LGA, Nigeria. *Natural resources research*, 29(6), 3771–3788. <https://doi.org/10.1007/s11053-020-09673-9>
- [21] George, N. J. (2021). Geo-electrically and hydrogeologically derived vulnerability assessments of aquifer resources in the hinterland of parts of Akwa Ibom State, Nigeria. *Solid earth sciences*, 6(2), 70–79. <https://doi.org/10.1016/j.sesci.2021.04.002>
- [22] Ibuot, J., Akpabio, G., & George, N. (2013). A survey of the repository of groundwater potential and distribution using geoelectrical resistivity method in Itu Local Government Area (LGA), Akwa Ibom State, southern Nigeria. *Open geosciences*, 5(4), 538–547. <https://doi.org/10.2478/s13533-012-0152-5>
- [23] Ibuot, J. C., George, N. J., Okwesili, A. N., & Obiora, D. N. (2019). Investigation of litho-textural characteristics of aquifer in Nkanu West Local Government Area of Enugu state, southeastern Nigeria. *Journal of african earth sciences*, 153, 197–207. <https://doi.org/10.1016/j.jafrearsci.2019.03.004>
- [24] Obianwu, V., George, N., & Udofia, K. (2011). Estimation of aquifer hydraulic conductivity and effective porosity distributions using laboratory measurements on core samples in the Niger Delta, Southern Nigeria. *International review of physics*, 5(1), 19–24.
- [25] Obiora, D. N., Ibuot, J. C., & George, N. J. (2016). Evaluation of aquifer potential, geoelectric and hydraulic parameters in Ezza North, southeastern Nigeria, using geoelectric sounding. *International journal of environmental science and technology*, 13, 435–444. <https://doi.org/10.1007/s13762-015-0886-y>
- [26] Ibanga, J. I., & George, N. J. (2016). Estimating geohydraulic parameters, protective strength, and corrosivity of hydrogeological units: a case study of ALSCON, Ikot Abasi, southern Nigeria. *Arabian journal of geosciences*, 9, 1–16. <https://doi.org/10.1007/s12517-016-2390-1>
- [27] Stempvoort, D. Van, Ewert, L., & Wassenaar, L. (1993). Aquifer vulnerability index: a GIS-compatible method for groundwater vulnerability mapping. *Canadian water resources journal*, 18(1), 25–37. <https://doi.org/10.4296/cwrj1801025>

- [28] Aweto, K. E. (2011). Aquifer vulnerability assessment at Oke-Ila area, southwestern Nigeria. *International journal of the physical sciences*, 6(33), 7574–7583.
- [29] Karadavut, S. (2009). *Potential and quality of surface water and ground water resources in aksaray province and their assessment in terms of efficient irrigation* [Thesis]. <https://ouci.dntb.gov.ua/en/works/4zkddMEI/>
- [30] Shamsudduha, M., Taylor, R. G., & Longuevergne, L. (2012). Monitoring groundwater storage changes in the highly seasonal humid tropics: Validation of GRACE measurements in the Bengal Basin. *Water resources research*, 48(2). <https://doi.org/10.1029/2011WR010993>
- [31] Petters, S. W. (1982). Central west African cretaceous-tertiary benthic foraminifera and stratigraphy. *Palaeontographica abt. A*, 179, 1–104. <https://doi.org/10.2343/geochemj.40.227>
- [32] Petters, S. W., Usoro, E. J., Udo, E. J., Obot, U. W., & Okpon, S. N. (1989). *Physical background, soils and landuse and ecological problems*. <https://www.sciepub.com/reference/13194>
- [33] GSN. (1962). *Nigerian geological map series, sheets 79 (Umuahia) and 82 (Calabar)*. <https://esdac.jrc.ec.europa.eu/content/umuahia-geological-series-nigeria-sheet-79>
- [34] Short, K. C., & Stauble, A. J. (1967). Outline of geology of Niger Delta. *AAPG bulletin*, 51(5), 761–779.
- [35] Tizro, A. T. (2002). *Hydrogeological investigations by surface geoelectrical method in hard rock formation—a case study*. <https://archives.datapages.com/data/geological-society-of-malaysia/bulletins/045/045001/pdfs/37.pdf>
- [36] Akpan, A. E., Ugbaja, A. N., & George, N. J. (2013). Integrated geophysical, geochemical and hydrogeological investigation of shallow groundwater resources in parts of the Ikom-Mamfe Embayment and the adjoining areas in Cross River State, Nigeria. *Environmental earth sciences*, 70(3), 1435–1456. <https://doi.org/10.1007/s12665-013-2232-3>
- [37] Thomas, J. E., George, N. J., Ekanem, A. M., & Nsikak, E. E. (2020). Electrostratigraphy and hydrogeochemistry of hyporheic zone and water-bearing caches in the littoral shorefront of Akwa Ibom State University, Southern Nigeria. *Environmental monitoring and assessment*, 192, 1–19. <https://doi.org/10.1007/s10661-020-08436-6>
- [38] Vander Velpen, B. P. A., & Sporry, R. J. (1993). RESIST. A computer program to process resistivity sounding data on pc compatibles. *Computers & geosciences*, 19(5), 691–703. [https://doi.org/10.1016/0098-3004\(93\)90102-B](https://doi.org/10.1016/0098-3004(93)90102-B)
- [39] Loke, M. H., & Barker, R. D. (1996). Rapid least-squares inversion of apparent resistivity pseudosections by a quasi-Newton method1. *Geophysical prospecting*, 44(1), 131–152. <https://doi.org/10.1111/j.1365-2478.1996.tb00142.x>
- [40] Loke, M. H., & Dahlin, T. (2002). A comparison of the Gauss–Newton and quasi-Newton methods in resistivity imaging inversion. *Journal of applied geophysics*, 49(3), 149–162. [https://doi.org/10.1016/S0926-9851\(01\)00106-9](https://doi.org/10.1016/S0926-9851(01)00106-9)
- [41] Loke, M. H., Acworth, I., & Dahlin, T. (2001). A comparison of smooth and blocky inversion methods in 2-D electrical imaging surveys. *ASEG extended abstracts*, 2001(1), 1–4. <https://doi.org/10.1071/EG03182>
- [42] Frohlich, R. K., & Kelly, W. E. (1988). Estimates of specific yield with the geoelectric resistivity method in glacial aquifers. *Journal of hydrology*, 97(1–2), 33–44. [https://doi.org/10.1016/0022-1694\(88\)90064-9](https://doi.org/10.1016/0022-1694(88)90064-9)
- [43] George, N. J., Akpan, A. E., & Akpan, F. S. (2017). Assessment of spatial distribution of porosity and aquifer geohydraulic parameters in parts of the Tertiary–Quaternary hydrogeoresource of south-eastern Nigeria. *NRIAG journal of astronomy and geophysics*, 6(2), 422–433. <https://doi.org/10.1016/j.nrjag.2017.09.001>
- [44] George, N. J., Ekanem, A. M., Thomas, J. E., & Ekong, S. A. (2021). Mapping depths of groundwater-level architecture: implications on modest groundwater-level declines and failures of boreholes in sedimentary environs. *Acta geophysica*, 69(5), 1919–1932. <https://doi.org/10.1007/s11600-021-00663-w>
- [45] Samouëlian, A., Cousin, I., Tabbagh, A., Bruand, A., & Richard, G. (2005). Electrical resistivity survey in soil science: a review. *Soil and tillage research*, 83(2), 173–193. <https://doi.org/10.1016/j.still.2004.10.004>
- [46] Onu, N. N. (2003). Estimates of the relative specific yield of aquifers from geo-electrical sounding data of the coastal plains of southeastern Nigeria. *Journal of technology and education in nigeria*, 8(1), 69–83. DOI:10.4314/joten.v8i1.35641
- [47] Fetter, C. (1994). *Applied hydrogeology*. Macmillan College Publishing Company.

- [48] Braga, A. C. de O., Malagutti Filho, W., & Dourado, J. C. (2006). Resistivity (DC) method applied to aquifer protection studies. *Revista brasileira de geofísica*, 24, 573–581. <https://doi.org/10.1590/S0102-261X2006000400010>
- [49] Niwas, S., & Celik, M. (2012). Equation estimation of porosity and hydraulic conductivity of Ruhrtal aquifer in Germany using near surface geophysics. *Journal of applied geophysics*, 84, 77–85. <https://doi.org/10.1016/j.jappgeo.2012.06.001>
- [50] Tripp, A. C., Hohmann, G. W., & Swift Jr, C. M. (1984). Two-dimensional resistivity inversion. *Geophysics*, 49(10), 1708–1717. <https://doi.org/10.1190/1.1441578>
- [51] Ekanem, A. M., George, N. J., Thomas, J. E., & Nathaniel, E. U. (2020). Empirical relations between aquifer geohydraulic–geoelectric properties derived from surficial resistivity measurements in parts of Akwa Ibom State, Southern Nigeria. *Natural resources research*, 29, 2635–2646. <https://doi.org/10.1007/s11053-019-09606-1>
- [52] Short, K. C., & Stauble, A. J. (1966). Outline of geology of Niger Delta. *AAPG bulletin*, 50(3), 634–635.
- [53] Ekanem, A. M. (2020). Georesistivity modelling and appraisal of soil water retention capacity in Akwa Ibom State University main campus and its environs, Southern Nigeria. *Modeling earth systems and environment*, 6(4), 2597–2608. <https://doi.org/10.1007/s40808-020-00850-6>
- [54] King, G. E., Wildt, P. J., & O'Connell, E. (2003). Sand control completion reliability and failure rate comparison with a multi-thousand well database. *SPE annual technical conference and exhibition?* (p. 84262). SPE. <https://doi.org/10.2118/84262-MS>
- [55] Vázquez-Báez, V., Rubio-Arellano, A., García-Toral, D., & Mora, I. R. (2019). Modeling an aquifer: Numerical solution to the groundwater flow equation. *Mathematical problems in engineering*, 2019(1), 1613726. DOI:10.1155/2019/1613726
- [56] Gheorghe, A. (1978). Processing and synthesis of hydrological data. *Abacus press junebridge wells, kent*, 290, 122–136.
- [57] Oladapo, M. I., Mohammed, M. Z., Adeoye, O. O., & Adetola, B. A. (2004). Geoelectrical investigation of the Ondo state housing corporation estate Ijapo Akure, Southwestern Nigeria. *Journal of mining and geology*, 40(1), 41–48. DOI: 10.4314/jmg.v40i1.18807